Research Article

Effect of Human Skin-Derived Stem Cells on Vessel Architecture, Tumor Growth, and Tumor Invasion in Brain Tumor Animal Models

Federica Pisati,[1,4] Marzia Belicchi,[1,4] Francesco Acerbi,[2,4] Chiara Marchesi,[1,4] Carlo Giussani,[2,4] Manuela Gavina,[1,4] Sophie Javerzat,[3,4] Martin Hagedorn,[3,4] Giorgio Carrabba,[2,4] Valeria Lucini,[2,4] Sergio Maria Gaini,[2,4] Nereo Bresolin,[1,4] Lorenzo Bello,[2,4] Andreas Bikfalvi,[3,4] and Yvan Torrente[1,4]

[1]Stem Cell Laboratory, Department of Neurological Science, Centro Dino Ferrari and [2]Unit of Neurosurgery, Fondazione Istituto di Ricovero e Cura a Carattere Scientifico Ospedale Maggiore Policlinico, University of Milan, Milan, Italy; [3]Institut National de la Sante et de la Recherche Medicale E0113 Molecular Mechanism of Angiogenesis, University of Bordeaux 1, Talence, France; and [4]European Laboratory for Angiogenesis and Translational Research, University Bordeaux and INSERM EMI 0113, Bordeaux, France and University of Milan, Milan, Italy

Abstract

Glioblastomas represent an important cause of cancer-related mortality with poor survival. Despite many advances, the mean survival time has not significantly improved in the last decades. New experimental approaches have shown tumor regression after the grafting of neural stem cells and human mesenchymal stem cells into experimental intracranial gliomas of adult rodents. However, the cell source seems to be an important limitation for autologous transplantation in glioblastoma. In the present study, we evaluated the tumor targeting and antitumor activity of human skin-derived stem cells (hSDSCs) in human brain tumor models. The hSDSCs exhibit tumor targeting characteristics *in vivo* when injected into the controlateral hemisphere or into the tail vein of mice. When implanted directly into glioblastomas, hSDSCs distributed themselves extensively throughout the tumor mass, reduced tumor vessel density, and decreased angiogenic sprouts. In addition, transplanted hSDSCs differentiate into pericyte cell and release high amounts of human transforming growth factor-β1 with low expression of vascular endothelial growth factor, which may contribute to the decreased tumor cell invasion and number of tumor vessels. In long-term experiments, the hSDSCs were also able to significantly inhibit tumor growth and to prolong animal survival. Similar behavior was seen when hSDSCs were implanted into two different tumor models, the chicken embryo experimental glioma model and the transgenic Tyrp1-Tag mice. Taken together, these data validate the use of hSDSCs for targeting human brain tumors. They may represent therapeutically effective cells for the treatment of intracranial tumors after autologous transplantation. [Cancer Res 2007;67(7):3054–63]

Introduction

Brain tumors, such as glioblastoma multiforme, are highly aggressive tumors and are characterized by marked angiogenesis and extensive tumor cell invasion into the normal brain parenchyma (1–3). To date, there are no efficient therapeutics available for glioblastoma multiforme. Surgical removal of the tumor, radiotherapy, and chemotherapy, including new drugs, such as temozolamide, improve survival for a certain period after which the tumor relapses. Therefore, the need to develop new effective therapeutic tools is particularly high. Therapeutics for glioblastoma multiforme ideally should aim to target both the tumor cell and the tumor vasculature (4–6). Many animal studies have shown that the tumor vasculature can be selectively targeted without affecting existing vessels (7, 8). This approach presents some advantages, one of which is that the tumor vasculature, derived from normal host cells, is less likely to develop therapeutic resistance (9, 10).

Recently, transplanted neural stem cells (NSCs) have been recognized for their ability to migrate throughout the central nervous system (11, 12). The tropism of NSCs for brain tumor can be used for delivering therapeutic molecules, such as genes, proteins, peptides, or small chemical molecules (13, 14). However, their clinical application is limited by ethical and logistic problems such as their isolation and their immunologic compatibility in allogenic transplantation. It therefore becomes mandatory to identify new sources of readily accessible stem cells with similar tumor targeting properties. Mesenchymal stem cells (MSC) can be easily isolated from the bone marrow (15, 16) and migrate after local intracranial delivery to human gliomas (17). Moreover, U87-MG glioblastomas grown in mice and treated marrow-derived neural competent cells transduced with soluble platelet-factor-4 (sPF4) showed a decrease in tumor growth (18). We isolated recently and characterized a multipotent stem cells from human skin tissue expressing the CD133, a hemapoietic/endothelial marker (19). These cells could represent a new source of accessible stem cells for tumor treatment. In this study, we undertook a series of experiments to investigate the tumor targeting capacity of human skin-derived stem cells (hSDSCs) in animal models of human glioblastoma. Our results indicate that hSDSCs indeed target brain tumors, inhibit tumor growth, and modulate the vessel architecture within tumors.

Materials and Methods

Cell culture. The human glioblastoma cell line U87-MG [American Type Culture Collection (ATCC), Manassas, VA] was used in all animal experiments. U87-MG were cultured in MEM-α (Life Technologies, Inc., Grand Island, NY) supplemented with 2 mmol/L L-glutamine, 2 mmol/L sodium pyruvate, 100 units/mL penicillin, 0.25 µg/mL streptomycin

fungizone, and 10% fetal bovine serum (FBS; Life Technologies). Cells were maintained in T-25 tissue culture flasks in 5% CO_2/95% air at 37°C in a humidified incubator and were routinely passaged at confluency. For the intracranial transplantation experiments, U87 cells were dispersed with a 0.05% solution of trypsin/EDTA (Life Technologies), washed with PBS, and adjusted to a final concentration of 5×10^4cells/10 μL in PBS. The porcine aortic endothelial cell line stably transfected with KDR (PAE/KDR; ATCC) was used as control for the migration experiments. These cells were cultured in Ham's F-12 medium with 10% FCS and 10 μg/mL geneticin (G-418 sulfate). Human adult skin tissues were obtained from 14 healthy volunteer donors (12–65 years of age) after obtaining informed consent for the guidelines of the University of Milan Committed on the Use of Human Subjects in Research. All the experiments were done with pooled cells from several donors. Skin tissues (ranging in the adult between 5 and 10 mm^3) were dissected carefully, without contamination from other tissues, and minced into smaller pieces with razor blades. Smaller pieces were washed thrice with essential balanced salt solution (EBSS) and enzymatically dissociated by adding 0.2% collagenase type I× and 0.1% trypsin for 1 h at 37°C followed by 0.1% DNase for 1 min at room temperature. The tissue cell extract was filtered with a 70-μm nylon mesh (DAKO, Carpinteria, CA) and plated in noncoated flask for 24 h. The growth medium used was composed of DMEM/F-12 (1:1) and 20% FBS, including HEPES buffer (5 mmol/L), glucose (0.6%), sodium bicarbonate (3 mmol/L), and glutamine (2 mmol/L). hSDSCs cells were resuspended in PBS, incubated with CD133 (monoclonal antibody)–conjugated super paramagnetic microbeads (CD133 Isolation kit, Miltenyi Biotec, Bergisch-Gladbach, Germany), washed, and processed by using a magnetic-activated cell sorter (MACS; Miltenyi Biotec). After selection, an aliquot of the CD133-positive cell fraction was analyzed by cytofluorimetry to assess purity. To verify whether hSDSCs can also differentiate into pericytes, these cells were plated in EGM2 medium (Cambrex) enriched with 10% FBS. After 7 days, cultured cells were stained for pericyte markers as alkaline phosphatase, CD146, NG2, α-smooth muscle actin (α-SMA), and desmin.

Endothelial progenitor cells (EPC) were obtained by blood-derived CD133-positive cell sorting for the CD34-APC (Becton Dickinson, Immunocytometry Systems, San Jose, CA), with a dual laser FACS-Vantage SE (Becton Dickinson, Immunocytometry Systems), to obtain a purified CD133-positive/CD34-positive population. Cells were cultured under the same conditions as described for hSDSCs. For tumor targeting studies, cells were labeled with PKH26 as described previously (20). For the short- and long-term transplantation, cells were transduced with a lentivirus expressing the green fluorescent protein (GFP) cDNA under the human phosphoglycerate kinase promoter (21). In all experiments, 30,000 cells diluted into 5 μL saline solution were injected.

Chick chorio-allantoic membrane experiments. Experimental glioma growth was obtained after grafting 3 million U87 cells in 20 μL of medium on the chorio-allantoic membrane (CAM) as described previously (22). For the first experiment, after 2 days of U87 growth, the tumor received 30,000 hSDSCs (n = 6) labeled with PKH red dye. For the second series of experiments, 120,000 of hSDSCs PKH red positive (n = 7) were used. Control experimental tumors were treated with cell-free medium (n = 9). Seven days after U87 implantation, tumors were removed and frozen in liquid nitrogen–cooled isopentane. Cryostat sections from frozen tissues embedded in ornithine carbamyl transferase (OCT) were cut into 8-μm serial sections and processed for immunolabeling.

Animal experiments. For the intracranial glioma model, 6-week-old nude mice (Charles Rivers Italia, Calco, Italy) received a stereotactical injection of 50,000 human U87 glioma cells into the left forebrain (2 mm lateral and 1 mm anterior to bregma, at a 3 mm depth from the skull surface). For tumor targeting experiments, the right hemisphere was injected with hSDSCs (n = 5), KDR (n = 5), or EPCs (n = 5) 21 days after the implantation of the U87 cell line into the controlateral hemisphere. After 3 and 14 days, mice were sacrificed and their brains were removed, embedded in OCT, and stored at −70°C. For the homing experiments, we injected i.v. 120,000 hSDSCs (n = 5) and EPCs (n = 5) into U87 implanted nude mice and sacrificed them after 21 days. For every experiment, the control group (n = 4) did not receive cells after tumor implantation. The

short- and long-term experiments were done in two different groups. In the first group of experiments, the hSDSCs (n = 20) were transplanted omolaterally into the 5-day implanted tumor. In the second group of experiments, hSDSCs (n = 32) were transplanted omolaterally 10 days after U87 cell line implantation. For short-term experiments, all animals were killed and their brains were removed 21 days after tumor implantation. For long-term experiments, animals were carefully monitored for the occurrence of any side effects and immediately sacrificed at the occurrence of any neurologic deficits. Control groups only received U87 injection (n = 21). Two groups of animal controls were represented by five males and four females not injected. The Tyrp1-Tag line was obtained from Dr. F. Beermann (Swiss Institute for Experimental Cancer Research, Lausanne, Switzerland). Tyrp1-Tag males develop a tumor from the retinal pigment epithelium and represent a good model for tumor invasion (22). hSDSCs were transplanted in males (n = 8) and control littermate females with no tumors (n = 4). All brains were fixed in 5% paraformaldehyde in PBS for 24 h at 4°C, dehydrated in 30% sucrose in PBS for 24 h at 4°C, embedded in OCT, and stored at −70°C. Brain tissues were cut on a cryostat into 7-μm serial sections and used for H&E staining or immunohistochemistry.

Immunohistochemical analysis. Sections were fixed in 80% ethanol for 3 min and then preincubated with 0.1% Triton X-100 and 10% horse serum for 30 min at room temperature. Primary antibodies were diluted in PBS containing 1% horse serum and then incubated for 2 h at room temperature. Polyclonal anti-GFP594 conjugate (GFP594; 1:50; Molecular Probes) was used to detect hSDSCs and human EPCs after brain transplantation. Tumor sections were incubated with anti-lamin A/C (1:100; Novocastra), anti-vimentin (1:100; Chemicon), anti-angiopoietin 2 (Ang2; 1:100; Chemicon), anti-fibronectin (1:100; Sigma-Aldrich, St. Louis, MO), and anti-collagen type IV (1:100; DAKO). Proliferating cells were detected by staining with human KI67 (1:100; DAKO). Apoptosis was detected by using terminal deoxynucleotidyl transferase–mediated dUTP nick end labeling staining (TUNEL; Roche) as described previously (23). For detection of pericyte coverage, double labeling experiments were done with monoclonal anti-CD31 (1:50; Becton Dickinson) and polyclonal anti-desmin (1:200; DAKO). Tumor vessels were immunostained with anti-CD31 and anti–von Willebrand factor (1:100; DAKO) or monoclonal anti-laminin (1:100; Sigma-Aldrich). Monoclonal antibodies anti-CD45 (1:100; RD Systems) and anti-CD133 (1:100; RD Systems) were used to detect human stem cells in the transgenic mice. Brain sections were also incubated with human endothelial markers as Ve-cadherin (1:50; Chemicon), α-SMA (1:100; Sigma-Aldrich), and angiopoietin 1 (Ang1; 1:100; RD Systems). The sections were rinsed in PBS and incubated with corresponding secondary antibodies Alexa Fluor 488, Alexa Fluor 594, or Alexa Fluor 647 (1:200; Molecular Probes), for 30 min a room temperature. For experimental glioma grown on the CAM, chick blood vessels were analyzed by using SNA-1 lectin FITC conjugated (1:200; Vector Laboratories, Burlingame, CA). Cell nuclei were stained with 4′,6-diamidino-2-phenylindole (DAPI), and sections were mounted with ProLong anti-Fade (Molecular Probes) and examined under a Leica DMIR2 fluorescence microscope. For the immunohistochemical staining, sections were incubated at room temperature for 20 min with a solution of methanol containing 0.03% H_2O_2 and incubated for 30 min with 1% horse serum and then for 1 h with the following antibodies: anti-CD31 (1:50) and anti-desmin (1:100, Novocastra). After a brief rinse with PBS, sections were incubated with biotinylated secondary antibodies (1:100; Vector Laboratories), washed, and incubated with the avidin-biotinylated peroxidase complex (avidin-biotin complex method kit, Vector Laboratories). The staining was visualized by treatment for 10 min in a 0.05% solution of 3,3′-diaminobenzidine and 0.01% H_2O_2 in 0.1 mol/L PBS. Sections were counterstained with hematoxylin. For all immunostaining, control reactions were done omitting the primary antibody, which was substituted by non immune serum.

Fluorescent *in situ* hybridization. Fluorescent *in situ* hybridization analysis was done on frozen brain tissue sections as described previously (24). The slides were first treated for 30 min with Histochoice Tissue Fixative (Sigma-Aldrich) and then dehydrated in 70%, 80%, and 95% alcohol. The denaturation was done at 70°C for 3 min in 70% deionized formamide

in 2 × SSC and slides were dehydrated again at −20°C. The hybridization was done overnight at 37°C in a moist chamber. A Cy-3–labeled human pan centromeric probe and FITC-labeled pan centromeric probe were used to identify human and mouse cells, respectively. The nuclei were counterstained with DAPI. Slides were observed using a Leica TCS 4D confocal microscope.

Western blot. To characterize the effects induced by the injection of hSDSCs cells, we evaluated the expression of several angiogenic factors by Western blot with anti-Ang1 (1:100; Santa Cruz Biotechnology, Inc. Santa Cruz, CA), anti-Ang2 (1:50; Santa Cruz Biotechnology), and anti–platelet-derived growth factor BB (1:200; Santa Cruz Biotechnology) as described previously (25).

Statistical analysis. Data are presented as means ± SD. Statistical analysis was carried out by the Student's *t* test. We considered probability (*P*) values <0.05 as significant.

Results

Effects of hSDSCs on the chicken embryo glioma model. To characterize the effects of hSDSCs on tumor angiogenesis, we evaluated these cells in the experimental glioma grown on the CAM of the chick embryo as described in diagram of Fig. 1*A*. In this model, U87 glioma cells form a solid tumor, which
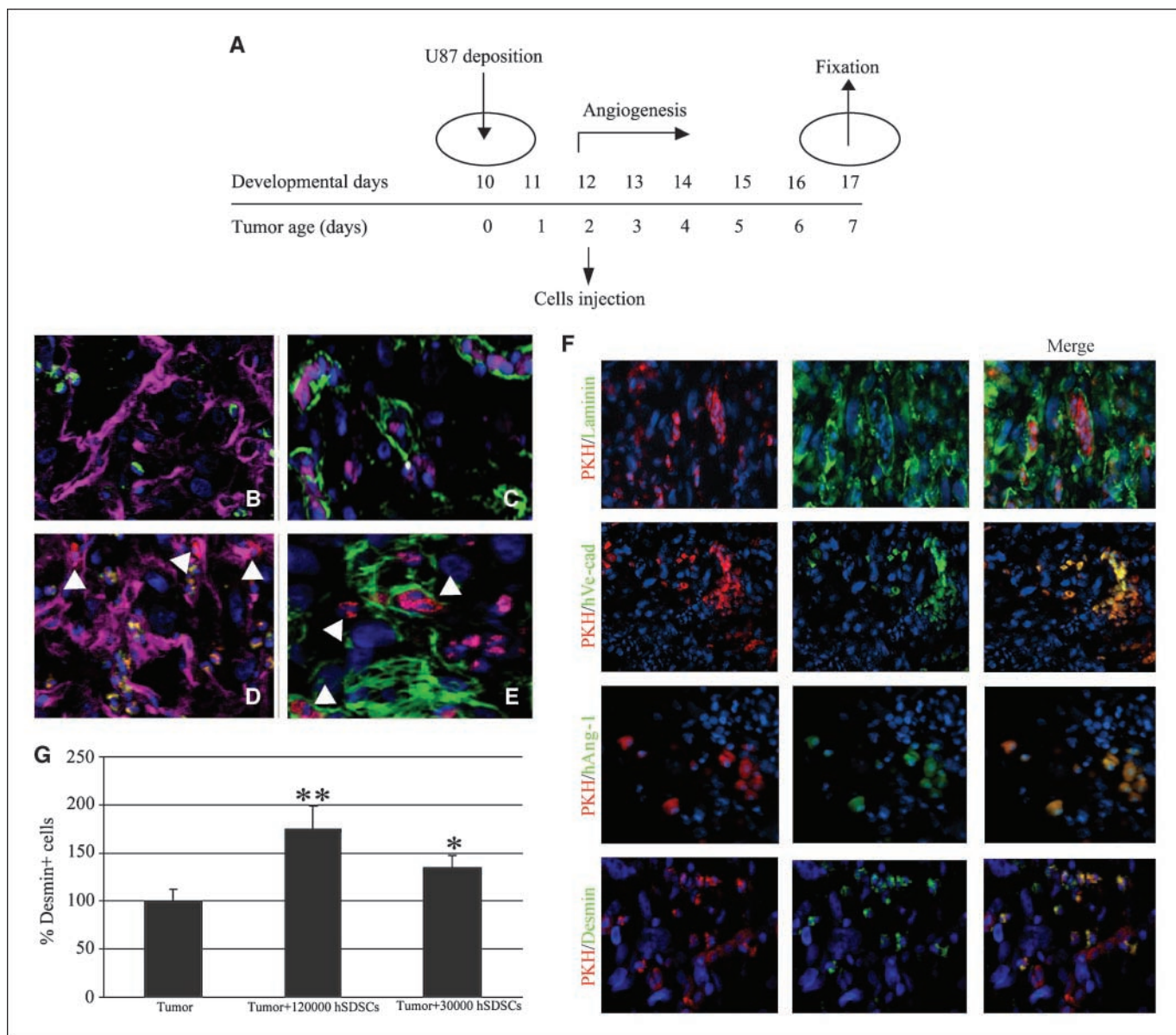
Figure 1. hSDSCs transplantation on a chicken embryo glioma model. Experimental glioma assay. *A,* 2 d after U87 implantation into CAM, 30,000 and 120,000 hSDSCs were injected on the tumor surface, and 5 d after cell injection, the CAM tissues were removed and frozen in liquid nitrogen–cooled isopentane. Biomicroscopy showed a progressive tumor vascularization at the surface of both tumors treated with 30,000 and 120,000 hSDSCs. *B,* 7 d after U87 injection, tortuous vessels, expressing the laminin antigen (Cy-5), with desmin-positive pericytes (*green*), were detected inside the tumor area. *C,* in these control tumors, only few desmin-positive pericytes (Cy-5) were found associated to α-SMA-positive vessels (*green*). *D,* after injection, PKH26-positive hSDSCs (*red, arrowhead*) distributed themselves around the laminin-positive vessels (Cy-5). *E,* labeled cells (*red*) coexpressing the desmin antigen (Cy-5, *arrowhead*) were also found associated to α-SMA-positive blood vessels (*green*). *F,* hSDSCs were also distributed as cellular clusters within the tumor area, coexpressing the PKH26 (*red*) and human Ve-cadherin (*green*), desmin (*green*), or Ang1. *G,* quantitative analysis of the number of pericytes desmin-positive cells. Data are representative of three experiments (seven eggs per group). *, *P* < 0.05; **, *P* < 0.001, statistical analysis (Student's two-tailed *t* test) proved the difference between control tumor and hSDSC-treated tumors.
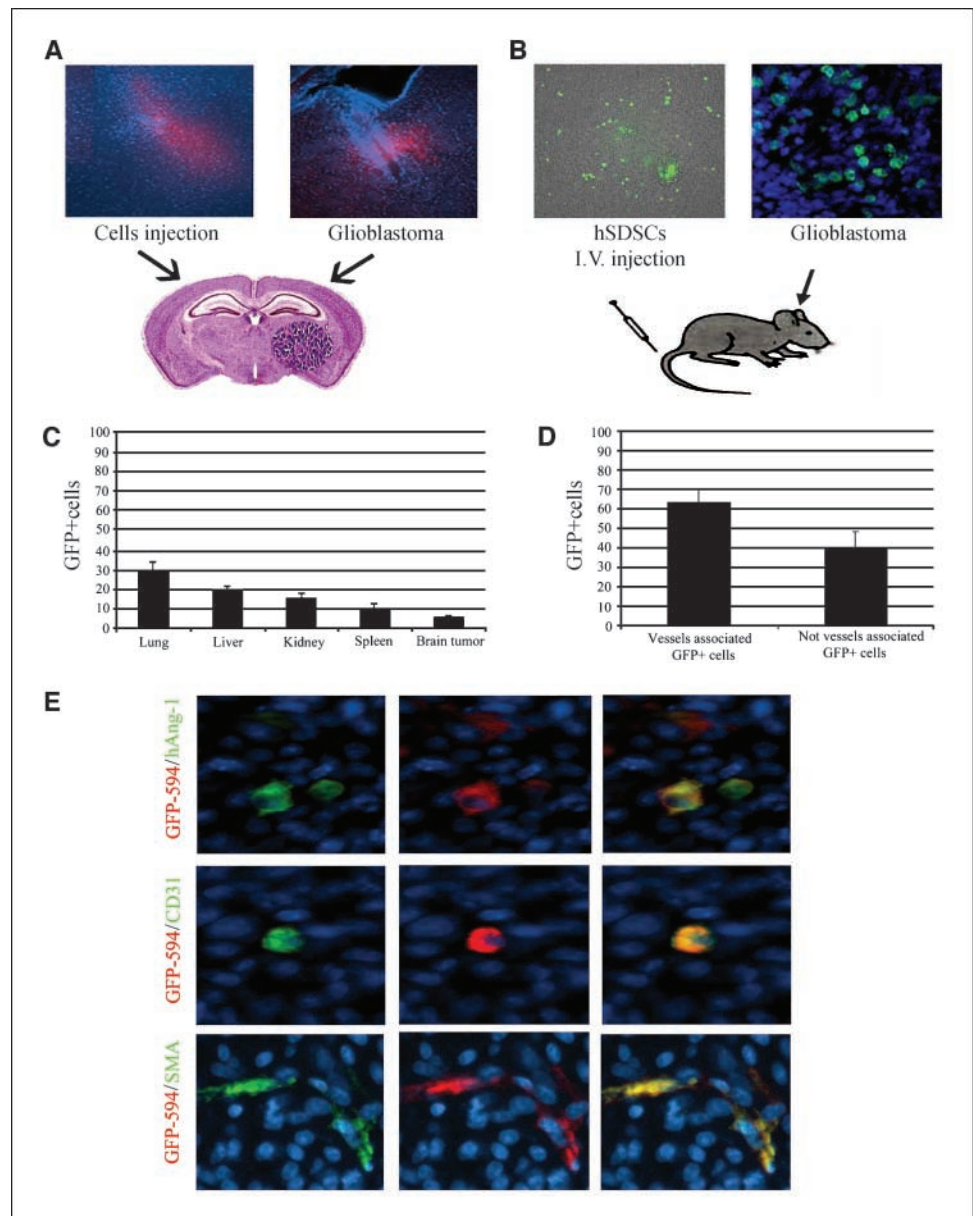
Figure 2. Tumor target ability of hSDSCs. *A,* below each photograph is a schematized composite image of the experimental model. The U87 human cells were implanted in the frontal lobe of nude mice and PKH26-positive hSDSCs were injected into the controlateral hemisphere. *Left,* red PKH26-positive hSDSCs counterstained with DAPI at the site of injection; *right,* several PKH26-positive red cells within the tumor area 14 d after the injection. *B,* to determine the tumor homing capacity, the transduced GFP594-positive hSDSCs (*left*) were injected into the tail vein of nude mice, in which a U87 glioblastoma had been established 14 d before. *Right,* a cluster of injected GFP594-positive hSDSCs within the tumor area 21 d after their i.v. transplantation. *C,* quantification of the i.v. injected GFP594-positive hSDSCs in different tissues, such as lungs, kidneys, liver, and brain tumor. *D,* quantitative analysis of the percentage of GFP594-positive cells associated and not associated to the tumor vessels. *E,* several GFP594-positive cells that reached the brain tumor coexpressed the human Ang1, CD31, and α-SMA endothelial markers (*green*). Data are representative of three experiments (five mice per group).

progressively becomes vascularized (22). hSDSCs were labeled with PKH26 and deposited onto the tumor 2 days after U87 transplantation. After 7 days, tortuous and dilated vessels were visible at the tumor surface of treated and untreated tumors (data not shown). Analysis of histologic sections by H&E staining did not reveal significant differences in size of treated or untreated tumors (data not shown). Laminin staining (Fig. 1*B*) was done to visualize tumor vessel network and only few of them exhibited desmin-positive associated pericytes. Few desmin-positive pericytes were also observed around SMA-positive vessels (Fig. 1*C*). PKH-positive hSDSCs were distributed near and far from the injection site within and around the tumor in all specimens. These data indicate that hSDSCs have a high migratory capacity. After injection, labeled hSDSCs were detected near the tumor vessels, where some of them, reminiscent of pericytes, coexpressed the desmin antigen (Fig. 1*D*). PKH26/desmin double-positive cells, reminiscent of pericytes, were also found associated with SMA-positive tumor vessels (Fig. 1*E*). However, the total

number of desmin-positive cells was significantly increased in the center of hSDSC-treated tumors (n = 10) compared with untreated tumors (n = 10; Fig. 1*G*). Moreover, injection of hSDSCs decreased vessel density in treated tumors (vessel density in control = mean 72.5% ± 15.4 SE; vessel density in hSDSCs treated = mean 41.6% ± 11.1 SE, n = 10).

Double-positive hSDSCs were distributed as cellular clusters around tumor cells, where they coexpressed PKH26 and endothelial markers, such as the human Ang1 and human Ve-cadherin (Fig. 1*F*). These data were also confirmed by immunoblot analysis of pooled single cells isolated by laser capture microscopy (n = 1,000; data not shown).

Pericyte differentiation of hSDSCs was also obtained by *in vitro* experiments as indicated in Materials and Methods. These experiments revealed a pericyte-like cell population that expressed NG2 (17 ± 2.7% of total cells), desmin (25 ± 4.7% of total cells), and α-SMA (19 ± 6.1% of total cells) after 7 days of differentiation of hSDSCs.

hSDSCs *in vivo* migrated toward glioblastoma after contro-lateral injection. To evaluate the tumor targeting properties of hSDSCs *in vivo*, intracranial xenografts of human U87 were established in the frontal lobe of nude mice as indicated in Materials and Methods. Twenty-one days after tumor cell implantation, hSDSCs (3×10^4 suspended in 10 μL PBS) were injected into the controlateral hemisphere of the same animal. As control, two groups of nude mice received respectively a controlateral injection of EPCs

or porcine aortic endothelial cells transfected with cDNA of vascular endothelial growth factor (VEGF) receptor-2 (KDR cells). Before injection, cells were labeled with PHK26. Animals were killed 3 and 14 days after cell injection and brains were analyzed. Three days after cell injection, clusters of PKH-positive hSDSCs were seen exclusively at the injection site. However, 14 days after cell injection, hSDSC PKH-positive cells were detected in the controlateral hemisphere and within the tumor (Fig. 2*A*). This indicates that hSDSCs migrated
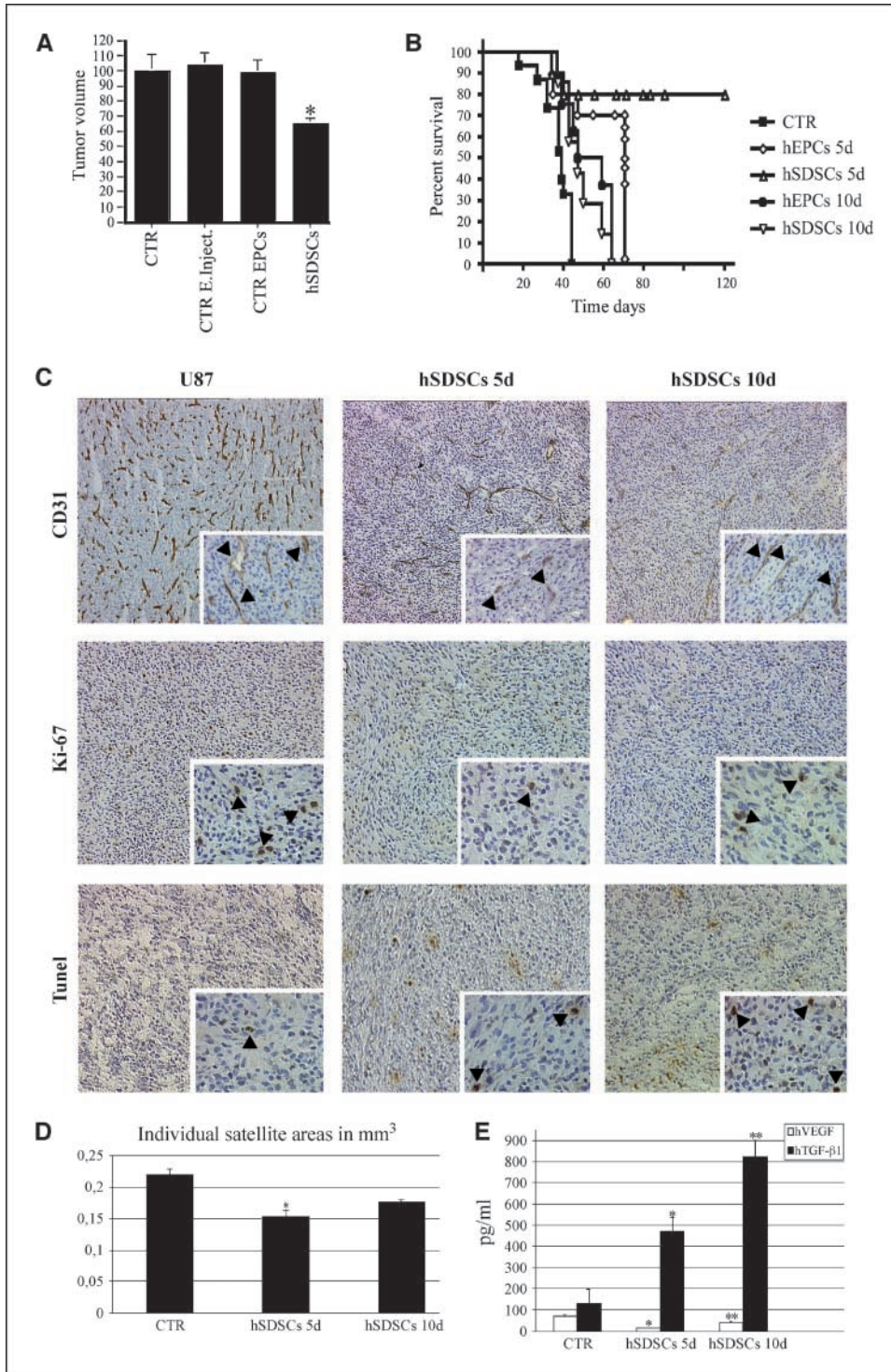
Figure 3. hSDSCs effect on tumor volume and animal survival. *A,* 21 days after hSDSCs transplantation of the animals, the tumor volume was calculated. The highest tumor growth inhibition was observed when we injected hSDSCs. *, $P < 0.05$. *Columns,* percentage of untreated tumor; *bars,* SE (referred as 100%). PBS-treated tumors and tumors injected with EP cells were also used as control. Data are representative of 20 mice for each group. Tumor volume was estimated using the formula for ellipsoid (width^2 × length) / 2. *B,* Kaplan-Meier survival curves. In long-term experiments, the brain tissues were harvested at the onset of signs of distress or neurologic deficits. The longest survival was observed when hSDSCs were injected 5 d (*5d*) after U87 transplantation. Data are representative of 20 mice for each group. Day 0 corresponds to the day of tumor cell implantation. *C,* histopathologic analysis of survival of treated animals after hSDSCs injection. The immunostaining with antibodies against CD31 was done to analyze the tumor vascular network: in the group of animals that received hSDSCs 5 d after the U87 implantation, the vessels appeared smaller with less capillary sprouts than the group treated 10 days (*10d*) after U87 implantation. Only in the survival animals that received the hSDSCs 5 d after the U87 implantation, we observed a reduction in the proliferation index, as shown by KI67 staining. In all survival animals, the apoptotic process, visualized by *in situ* labeling fragmented DNA (TUNEL), seemed higher than the untreated U87 implanted animals. The individual satellite area (*D*) was reduced compared with untreated tumor control. *, $P < 0.05$. The values were expressed as mean of three independent microscopic fields for tissue section. Magnification, ×40. The ELISA analysis from the tumor extracts (*E*) shows high expression of human TGF-β1 in hSDSC-transplanted tumors. Importantly, the VEGF expression is lower than untreated tumor control after hSDSCs transplantation (*E*). Data are representative of 24 mice from each group. *, $P < 0.05$; **, $P < 0.001$, statistical analysis (Student's two-tailed *t* test) proved the difference between control tumor and hSDSCs treated tumors.
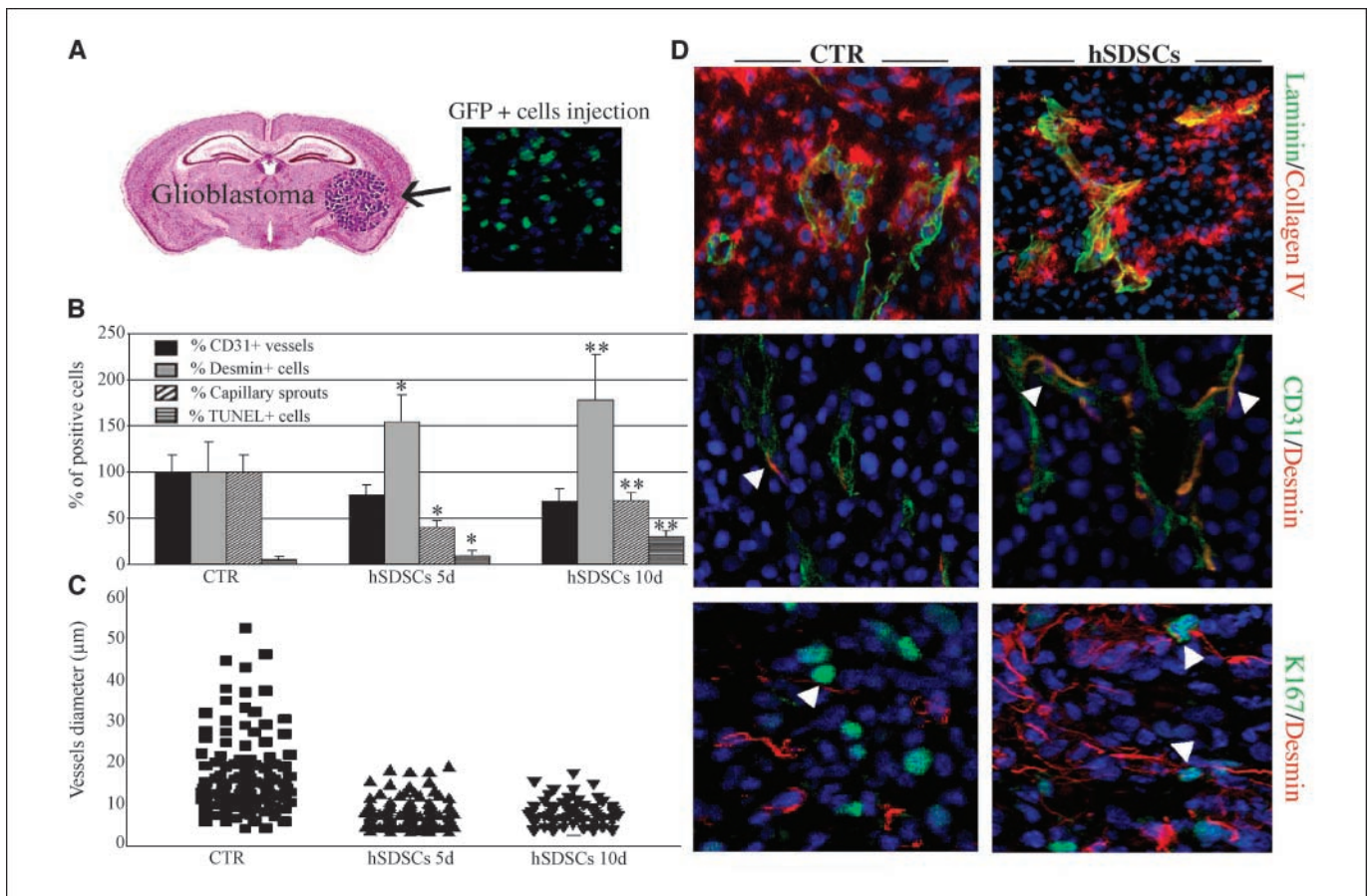
Figure 4. Characterization of tumors injected with GFP-positive hSDSCs and controls. *A,* schematized composite image of hSDSC implantation in U87 brain tumor in mice. Five days after tumor implantation, 30,000 GFP-positive hSDSCs were injected inside the tumor and visualized after 21 d (*left*). *B* and *C,* quantification of desmin-, CD31-, TUNEL-positive cells and vessel diameter in control or hSDSC-treated tumors. The number of desmin-, CD31-, and TUNEL-positive cells was expressed as mean of six independent microscopic fields for tissue section. Magnification, ×40. *, $P < 0.05$; **, $P < 0.001$, statistical significance, Student's two-tailed *t* test. Tumor vessel diameter quantification (*C*). The values of vessel diameter, expressed in micrometer, were obtained using NIH Image 63 and GraphPad Prism version (GraphPad Software, San Diego, CA): for each experimental group, individual vessel diameter is displayed as the same symbol: *square,* control tumor; *triangle,* hSDSC-treated tumors (5 d); *inverse triangle,* hSDSC-treated tumors (10 d). *D,* immunofluorescent images after double labeling of control (*CTR*) or hSDSC-treated tumors. Slides from control or hSDSC-treated tumors are double labeled with antibody against laminin/collagen IV, CD31/desmin, or K67/desmin and analyzed by confocal microscopy. The staining for type IV collagen showed a reduced expression in hSDSC-treated tumors compared with control tumors. Staining for desmin expression revealed a reduced number of pericytes within and around the tumor vessels in control tumors (*arrowhead*) versus hSDSC-treated tumors (*arrowhead*). None of them was Ki67 positive (*arrowhead*). Desmin-positive cells coexpressing the Ki67 antigen were seen after hSDSCs transplantation (*arrowhead*). Data are representative of four experiments (24 mice per group).

from the injection side across the corpus callosum and to the tumor. On the contrary, EPCs or KDR cells fail to migrate away from the injection site (data not shown).

hSDSCs target experimental glioblastoma after i.v. injection. To further determine the tumor targeting ability of hSDSCs, cells were injected into the tail vein of nude mice, in which U87 glioblastoma had been established 14 days before in the frontal lobe. As a control, we also injected EPCs. To distinguish injected cells from human cells migrating away from the tumor mass, they were transduced with a vector containing the GFP cDNA before injection (Fig. 2*B*). Twenty-one days after tumor cell implantation, a small percentage of injected hSDSCs ($\cong$ 5%) reached the brain tumor, whereas most cells that had probably passed through the capillary network ended in the venous circulation and were trapped in filter organs (Fig. 2*C*). hSDSCs and EPCs (data not shown) migrated to the tumor and interspersed throughout the tumor (Fig. 2*B*). Few GFP-positive hSDSCs were localized in the interface of the tumor mass, where they remained CD133 positive (data not shown). Throughout the tumor mass, we found hSDSCs

expressing Ang1, CD31, and α-SMA (Fig. 2*E*). The percentage of hSDSCs associated to laminin-positive vessels was about 61 ± 9% (Fig. 2*D*). Similarly, GFP-positive EPCs, when injected in mice, also expressed endothelial cell markers within the center of the tumor (data not shown).

Effects of hSDSCs after intratumoral cell implantation. For these experiments, cells were injected 5 and 10 days after U87 implantation homolaterally to the tumor. Brains were analyzed after 21 days (short-term experiments) or in long-term experiments for survival. After 21 days, a reduction of 40% in tumor size was seen in mice homolaterally injected with hSDSCs (Fig. 3*A*). In long-term experiments, untreated animals showed a survival of 50% after 28 days. Animals treated with hSDSCs reached 80% survival at 120 days (Fig. 3*B*). The majority of hSDSCs were interspersed throughout the tumor and only few cells were able to migrated to the periphery of the tumor mass (Fig. 4*A*). Angiogenesis in tumors was estimated by CD31 and desmin staining (Figs. 3*C* and 4*B* and *D*). In control mice implanted with tumor cells alone, large tortuous vessels with irregular diameter were detected (Fig. 4*C*).

In tumors of mice injected with hSDSCs, vessel number was decreased with smaller vessels of less variable size (Figs. 3*C* and 4*B* and *C*). A more detailed analysis revealed that there was less capillary sprouts and a reduction of teleangiectatic or dilated vessels in the animals that received the hSDSCs 5 days after U87 implantation (data not shown). Apoptotic indexes, quantified *in situ* by labeling fragmented DNA (TUNEL), were increased in tumors of animals that received hSDSCs 5 or 10 days after U87 implantation (Figs. 3*C* and 4*B*). Survival animals that received the hSDSCs 5 days after the U87 implantation showed a reduction in

the proliferation index, as shown by KI67 staining (Fig. 3*C*). Double labeling with anti-desmin and CD31 antibodies was done to visualize vessel-associated pericytes. In control tumors, only few vessels exhibited vessel-associated pericytes (Fig. 4*B* and *D*). In tumors from mice injected with hSDSCs, the percentage of desmin-positive cells was increased (80% ± 12.5 SE in SDSCs-injected mice versus 51.4% ± 9.8 SE in control mice; Fig. 4*B* and *D*). The increase of desmin-positive cells was accompanied by a reduction of CD31-positive vessels (Fig. 4*B*). Double staining for desmin and human KI67 in tumors from hSDSCs-injected mice
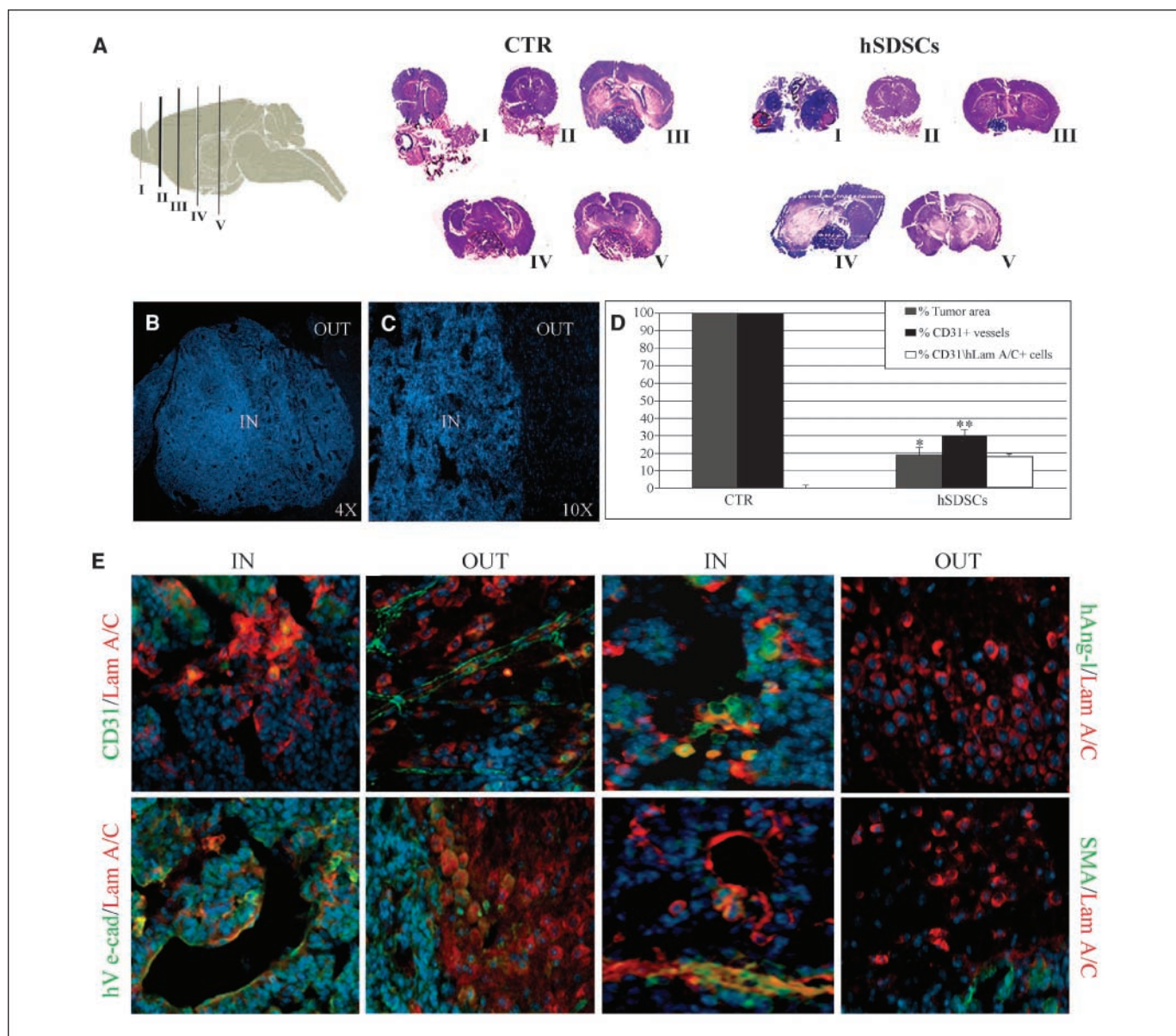
Figure 5. hSDSC implantation in tumors from Tyrp1-Tag transgenic mice. The hSDSCs were injected into the brains of tumor-bearing Tyrp1-Tag mice. *A,* schematic depiction of mouse brain showing the location of sections (*I–V*) used for the H&E staining of the brain of treated Tyrp1-Tag mice 45 days after the injections of hSDSCs. *Right,* H&E staining of tumor area of sections I to V with the reduction of the tumor size and invasion of treated Tyrp1-Tag mice (*hSDSCs*) versus control untreated tumor (*CTR*). *B* and *C,* two different magnification of DAPI staining for the selected areas of (*E*). *IN* and *OUT,* the center and the border of the tumor, respectively. *D,* the number of CD31-positive (total vessels) and CD31/lamin A/C double-positive vessels (human vessels). *n* = 6 independent fields. **, *P* < 0.001, statistical significance, Student's two-tailed *t* test. *E,* implanted hSDSCs were revealed by specific antihuman lamin A/C (*red*) and examined for the expression of human Ang1, CD31, human Ve-cadherin, and α-SMA (all shown in *green*) at the center (*IN*) and at the border of the tumor (*OUT*). Immunofluorescence analysis showed CD31 and human Ve-cadherin expression in hSDSCs-treated tumors. hSDSCs express human Ang1 in the center of the tumor mass. Data are representative of two experiments (five mice per group).

revealed the presence of few proliferating pericytes (Fig. 4*B* and *D*). Furthermore, staining for type IV collagen showed a reduced expression in hSDSCs-treated tumors compared with control tumors (Fig. 4*D*).

It is important to note that, in all experimental groups, injected cells never became tumorigenic. To show this behavior, for each experimental group, nude mice were engrafted with only human stem cells, and animals were sacrificed after 21 (as in short-term experiments) and 120 days (the longest survival observed in long-term experiments). In these experiments, injected hSDSCs never formed a nodule or a tumoral mass and, as recently described (19), these cells were localized as a small clusters to the host vessels and near the ventricular zone.

Intratumoral gliosis in SDSC-treated tumors is correlated to high expression of human transforming growth factor-β1. We observed a less invasive pattern of tumor growth in mice treated with hSDSCs compared with control groups. In fact, a reduced number of satellite tumor clustered around the primary was observed after hSDSCs (Fig. 3*D*). These satellites contained central vessel cores and their quantification revealed that their frequency was less in hSDSCs treated tumors than in U87-derived controls (Fig. 3*D*). We hypothesized that hSDSCs would induce a gliotic reaction and allowing the reduction of satellite tumor outgrowth. Gliotic reaction was quantified on histologic sections after staining for Azan Mallory, which labels fibrosis (data not shown). Sections from hSDSC-treated tumors revealed variable intratumoral gliotic areas around satellites (ranging from 9% to 1% of tumor volume) but the increase of these areas compared with untreated controls was not statistically significant (data not shown). One potential source for the increased gliosis and decreased number of vessels within the U87-derived tumor could be the secretion of human transforming growth factor-β (TGF-β) 1 by the hSDSCs. To screen for presence of secreted human TGF-β1, we did ELISA analysis from the supernatants of hSDSCs and from the transplanted tumors. ELISA analysis shows the presence of human TGF-β1 in both U87 (455.2 ± 103 SE pg/mL) and hSDSCs (308.7 ± 60 SE pg/mL) conditioned medium (data not shown). Importantly, we observed higher levels of TGF-β1 expression in transplanted tumors than in hSDSCs conditioned medium, up to 2- to 3-fold higher than in conditioned medium of hSDSCs or U87 cells (Fig. 3*E*). We also found higher expression of human TGF-β1 in tumors implanted with hSDSCs than in control tumors not implanted with hSDSCs (Fig. 3*E*). Moreover, VEGF expression was absent in hSDSCs conditioned medium and lower in tumors implanted with hSDSCs than in untreated control tumors (Fig. 3*E*). The ratio of TGF-β1/VEGF is highly in favor of TGF-β1 in both hSDSCs supernatants and tumor extracts. These findings suggested that transplanted hSDSCs release high amounts of human TGF-β1 with low expression of VEGF, which may contribute to the decreased tumor cell invasion and number of tumor vessels.

hSDSCs reduced tumor growth after injection into the brain of Tyrp1-Tag transgenic mouse. To confirm the capacity of hSDSCs to reduce the brain tumor outgrowth, we investigated their tumor targeting and antitumor activity in the Tyrp1-Tag transgenic mouse model. These mice develop highly aggressive tumors from the retinal pigmented epithelium of the eye that migrate along the optic nerve and invade the brain (26–28). These tumors are highly vascularized with blood vessels of heterogeneous size and shape and a discontinuous CD31-positive cell coverage. Male but not female mice develop tumors. PKH26-

labeled hSDSCs were injected into the cerebral hemisphere of male and females mice at postnatal day 21. Brains of tumor-bearing (males) or control mice (females) were analyzed at postnatal day 45. In control mice, clusters of PKH red–positive cells coexpressing the CD31 were found adjacent to reactive host GFAP-positive astrocytes (data not shown). We also found several PKH red–positive cells coexpressing desmin associated with brain blood vessels (data not shown). These data suggested vessel differentiation ability of hSDSCs when injected into the brain. In tumor-bearing male mice, hSDSCs injection was associated with an 80% ± 11 SE reduction of brain tumor area (analyzed from serial H&E-stained serial sections; *n* = 10; Fig. 5*A* and *D*). PKH red–positive cells were found in the periphery and within the tumor mass (data not shown). Furthermore, implanted cells were detected using a specific human lamin A/C antibody that only recognizes human cells (Fig. 5). Lamin A/C–positive hSDSCs were found at the interface of the tumor mass expressing the CD133 stem cell marker. hSDSCs around the tumor, as evidenced by counting lamin A/C–positive cells, were abundantly detected. Moreover, throughout the i.c. tumor mass, hSDSCs were found, which also expressed human Ang1 and Ve-cadherin (Fig. 5*E*). Around vessels, human CD31- and SMA-positive cells were also detected, whereas no expression of human Ang1 was seen (Fig. 5*E*). We also counted the number of CD31-positive vessels and the number of CD31/lamin A/C double-positive cells within the tumor mass. These data indicated a decrease of CD31-positive vessels after hSDSCs injection. However, the number of vessels of human origin (CD31/lamin A/C double-positive vessels) was higher than vessels expressing murine CD31 only (Fig. 5*D*). Furthermore, injection of hSDSCs was significantly associated with a decrease in the ability of tumor cells to invade normal brain (data not shown).

Discussion

In this study, we have evaluated the effects of hSDSCs on brain tumor targeting and development using three different experimental systems, the experimental glioma in the chicken CAM, U87 xenografts and the Tyrp-1Tag transgenic mice. These studies indicate that hSDSCs have a high capacity to migrate around and into experimental tumors, to partially acquire a vascular phenotype, and to impair tumor development by decreasing tumor-associated angiogenesis and invasion and by inducing tumor gliosis. The high migratory capacity of hSDSCs was first evidenced in the experimental glioma in the chicken CAM. This model mimics glioma development as it happens in patients within a short time-frame and has been validated by gene profiling studies (22). In these experiments, hSDSCs, deposited on the top of the glioma after 2 days of glioma development, were able to migrate around and inside the tumor. When injected controlaterally or i.v. in tumor-bearing nude mice, hSDSCs are able to localize into and around experimental tumors. To reinforce this contention, we have used the transgenic Tyrp-Tag mice that develop a highly aggressive tumor derived from the RPE that invades the brain. In this experimental setting, hSDSC cell injected along the optic nerve, also localize around and within the tumor mass. This indicates that the capacity for integration into tumors is an intrinsic property of these stem cells as it has been described previously for other types of stem cells (11, 15, 16). This is also in agreement with initial work from our group that showed high migratory capacity of hSDSCs into

the adult mouse brain (19). By combining the use of antibodies against human lamin A/C and labeled stem cells, or of stem cells transduced with GFP, it was possible to track the fate of injected cells. This method unambiguously recognizes that a fraction of transplanted cells partially localizes to CD31-positive tumor vessels.

hSDSCs exhibit vascular cell differentiation capacity when localized into the tumor tissue. First, labeling with anti-CD31 of a fraction of hSDSCs, localized to tumor blood vessels, indicates ability to differentiate into endothelial cells. This agrees with previous results that showed endothelial cell differentiation capacity of hSDSCs when injected into the normal mouse brain (19). Second, hSDSCs also exhibit pericyte/stroma cell differentiation ability *in vitro* and when implanted into tumor tissue in the brain. For example, hSDSCs exhibit pericyte differentiation capacity in culture in the presence of pericyte differentiation medium. Furthermore, only in nude mice engrafted with U87 glioma and injected with hSDSCs, several human lamin A/C (that is only expressed in human cells)–positive cells also expressed desmin and SMA. It is, at present, not clear whether hSDSCs significantly contribute to an increase in pericyte recruitment through its differentiation capacity. In addition, hSDSCs may release pericyte attraction factors, such as TGF-β (see below), and thus indirectly contribute to pericyte recruitment. Nevertheless, the vessel architecture after hSDSC treatment is modified and is composed of small elongated vessels, with small diameter, and better pericyte coverage, findings consistent with a normalization of tumor vessel architecture.

Tumor growth and invasion are strongly inhibited in the nude mice glioma model and the Tyrp-Tag mice but not in the experimental glioma in the CAM. The lack of effect on these variables is probably due to the short-time interval required for CAM experiments, which will mask potential inhibitory effects. Inhibition of tumor cell invasion, evidenced by a reduction of tumor satellites in hSDSC-treated tumors, was associated with an increase of expression of human TGF-β1. It is interesting to note that hSDSCs exhibit high capacity to proliferate in response to TGF-β1 (29). Although known for its growth-inhibitory function in epithelial tissues, high levels of TGF-β1 were correlated with tumor-suppressive function (30–33). Although the levels of TGF-β1 were highly increased in tumors treated with hSDSCs, much lower VEGF levels were observed. This indicates that the balance between VEGF and TGF-β is in favor of TGF-β that may counteract the effect of VEGF. In fact, TGF-β increases the expression of protease inhibitors, such as plasminogen activator inhibitor-1, thus counteracting extracellular proteolysis, thus inhibiting fibrin and collagen I degradation (34). On the contrary, VEGF favors extracellular proteolysis. Taken together, these results indicate that hSDSCs modify the growth factors repertoire in treated tumors leading to impairment of tumor development through the inhibition of angiogenesis and tumor cell invasion.

One can only speculate about the increase in survival when hSDSCs are injected 5 days after tumor implantation but not 10 days after tumor implantation. At 5 days, the effect of hSDSCs on tumor development occurs at an early phase of tumor expansion when tumor cells are bearly established in their tumor microenvironment. Apparently, hSDSCs are blocking signaling events that are critical for tumor expansion at this early phase of tumor development. This situation is somehow comparable with the effect of some antiangiogenesis molecules in experimental tumors where they are improving overall survival only when given from the beginning of the experiment ("angioprevention and angioinhibition") but not when they are administered at a later time point. To ascertain that the effects of hSDSCs were not dependent on the immunodeficient background of nude mice, experiments with immunocompetent Tyrp-Tag mice were done. Similarly, inhibition of tumor development was also observed in these mice. The antitumor activity is most likely not due to an activation of the antitumor immunoresponse in these mice and this for several reasons. First, we did not detect infiltration of immune cells in the vicinity of implanted hSDSCs. Second, low immunogenicity and absence of rejection as allowgrafts of stem cells, such as NSCs, were observed (35, 36). Third, we expanded hSDSCs using stem cell mitogens as indicated in Material and Methods. It has been reported that immunogenicity of porcine neural cell suspensions used for i.c. xenotransplantation is reduced when stem cell mitogens are used to expand precursor cells (37). Several arguments are in favor of an advantage of the use of hSDSCs when compared with other cell therapy–based strategies. Previous studies have shown the capability of NSCs obtained from neonatal mouse cerebellar germinal zone to target the tumor. Aboody et al. (12) showed that transplanted NSCs have the ability to migrate toward an intracranial tumor cell mass. This ability of stem cells to migrate toward a tumor mass was seen when injected at intracranial sites distant from the tumor and even after injection into the tail vein. This extensive migratory capacity of NSCs is retained in the tumor environment and may be advantageously applied both to delivering therapeutic molecules to the primary tumor and to distant sites from the central tumor mass. Recently, Benedetti et al. (11) reported that NSCs genetically modified to produce interleukin-4 could promote tumor regression and prolonged survival in mice that have been injected intracranially with the GL261 mouse glioma cell line. However, the inaccessibility of NSCs severely limits their clinical use. Bone marrow–derived MSCs represent an alternative source in the treatment of glioblastoma. This renewable population is particularly attractive for clinical uses because it can be easily obtained from the same patients and be used in allogenic transplantation, without immunosuppression, sometimes particularly problematic for the patient. Moreover, Nakamizo et al. (17) showed that human bone marrow MSCs migrated toward glioma after intracranial and intravascular injection. However, only engineered human MSCs (hMSC) have shown therapeutic advantages. After the intracranial injection of hMSCs transfected with an adenoviral vector containing the c-DNA of *INF-β* gene, treated animals had a significantly extended survival. On the contrary, control animals that received control hMSC–β-galactosidase had a shorter survival times than animals who received only the PBS solution. In fact, hMSCs may integrate into the glioblastoma and contribute to the mesenchymal elements of the tumors. It has been shown that bone marrow also represents an important source of EPCs (38). After injection, EPCs showed a high migratory capacity and presented a high tropism for the neovasculature, as shown in animal models of ischemia and of solid tumors (23, 39). Otherwise, when injected into animal tumor models, EPCs can incorporate themselves into the host vessels and increase the angiogenesis, with a consequent increase of blood supply, crucial for the tumor growth and the metastasis. However, when injected into the brain, EPCs are not able to migrate toward brain tumors in experimental brain tumor models (our observations in this study). hSDSCs have the advantages but not the

disadvantages of the cell therapy–based strategies described above. hSDSCs are an easily accessible cell population for autologous transplantation and have a high migratory capacity toward brain tumors. They are easily expandable *in vitro* and ~ 1,500,000 cells can be obtained after the third passage. They have differentiation capacity and are able to localize around the tumor and to migrate into the tumor when injected both into the brain and i.v. They can be transduced with vectors encoding for antitumor molecules (i.e., antiangiogenesis, anti-invasion, or proapoptotic/cytotoxic molecules). Thus, they constitute an ideal source for the development of novel cell-based therapies. Taken together, our results indicate that hSDSCs target brain tumors and have significant effects on brain tumor development and animal survival. HSDSCs constitute an ideal source for autologous transplantation in patients with glioblastoma and thus may help to overcome the limitations of other cell therapy–based approaches.

References

1. Walker AE, Robins M, Weinfeld FD. Epidemiology of brain tumors: the national survey of intracranial neoplasms. Neurology 1985;35:219–26.
2. Surawicz TS, David F, Freels S, Laws ER, Jr., Mench HR. Brain tumor survival: results from the National Cancer Data Base. J Neurooncol 1998;40:151–60.
3. Schiffer D, Cavalla P, Dutto A. Cell proliferation and invasion in malignant gliomas. Anticancer Res 1997;17:61–70.
4. Ferrara N. Vascular endothelial growth factor as a target for anticancer therapy. Oncologist 2004;9 Suppl 1:2–10.
5. Gasparini G, Longo R, Toi M, Ferrara N. Angiogenic inhibitors: a new therapeutic strategy in oncology. Nat Clin Pract 2005;2:562–77.
6. Gee Ms, Koch CJ, Evans SM, et al. Hypoxia-mediated apoptosis from angiogenesis inhibition underlies tumor control by recombinant interleukin 12. Cancer Res 1999;59:4882–9.
7. Folkman J. Anti-angiogenesis: new concept for therapy of solid tumors. Ann Surg 1972;75:409–16.
8. Neri D, Bicknell R. Tumor vascular targeting. Nat Rev Cancer 2005;5:436–46.
9. Kerbel RS. Inhibition of tumor angiogenesis as a strategy to circumvent acquired resistance to anticancer therapeutic agents. Bioessay 1991;13:31–6.
10. Boehm T, Folkman J, Browder T, O'Reilly MS. Anti-angiogenic therapy of experimental cancer does not induce acquired drug resistance. Nature 1997;309:404–7.
11. Benedetti S, Pirola B, Pollo B. Gene therapy of experimental brain tumor using neural progenitor cells. Nat Med 2000;6:447–50.
12. Aboody KS, Brown A, Rainov NG. Neural stem cells display extensive tropism for pathology in adult brain: evidence from intracranial glioma. PNAS 2000;97:12846–51.
13. Ehtesham M, Kabos P, Gutierrez MA. Induction of glioblastoma apoptosis using neural stem cells mediated delivery of tumor necrosis factor-related apoptosis-inducing ligand. Cancer Res 2002;62:7170–4.
14. Ehtesham M, Kabos P, Kabosova A, Neuman T, Black KL, Yu JS. The use of interleukin 12-secreting neural stem cells for the treatment of intracranial glioma. Cancer Res 2002;2062:7170–4.
15. Tocci A, Forte L. Mesenchymal stem cell: use and perspectives. Hematol J 2003;4:92–6.

16. Conget PA, Minguell JJ. Adenoviral-mediated gene transfer into *ex vivo* expanded human bone marrow mesenchymal progenitor cells. Exp Hematol 2000;28:382–90.
17. Nakamizo A, Marini F, Amano T, et al. Human bone marrow-derived stem cells in the treatment of gliomas. Cancer Res 2005;65:3307–18.
18. Lee J, Elkahloun AG, Messina SA, et al. Cellular and genetic characterization of human adult bone marrow-derived neural stem-like cells. A potential antiglioma cellular vector. Cancer Res 2003;6:8877–89.
19. Belicchi M, Pisati F, Porretti L, et al. Human skin-derived stem cells migrate throughout forebrain and differentiated into astrocytes after injection into adult mouse brain. J Neuros Res 2004;77:475–86.
20. El Fahime E, Torrente Y, Bresolin N, Tremblay JP. *In vivo* migration of transplanted myoblasts requires matrix metalloproteinase activity. Exp Cell Res 2001;258:279–87.
21. Sampaolesi M, Torrente Y, Innocenzi A, et al. Cell therapy of α-sarcoglycan null dystrophic mice through intra-arterial delivery of mesoangioblasts. Science 2003;25:487–92.
22. Hagedorn M, Javerzat S, Gilges D, et al. Accessing key steps of human tumor progression *in vivo* by using an avian embryo model. Proc Natl Acad Sci USA 2005;102:1643–8.
23. Asahara T, Masuda H, Takahashi T, et al. Bone marrow origin of endothelial progenitor cells responsible for postnatal vasculogenesis in physiological and pathological neovascularization. Circ Res 1999;85:221–8.
24. Gavrieli Y, Sherman Y, Ben-Sasson SA. Identification of programmed cell death *in situ* via specific labelling of nuclear DNA fragmentation. J Cell Biol 1992;119:493–501.
25. Torrente Y, Tremblay JP, Pisati F, et al. Intraarterial injection of muscle-derived CD34+Sca-1+ stem cells restores dystrophin in mdx mice. J Cell Biol 2001;152:335–41.
26. Rousseau B, Larrieu-Lahargue F, Javerzat S, Guilhem-Duclèon F, Beermann F, Bikfalvi A. The tyrp1-Tag/tyrp1-1-DN bigenic mouse: a model for selective inhibition of tumor development, angiogenesis, and invasion into the neural tissue by blockade of fibroblast growth factor (FGF) receptor activity. Cancer Res 2004;64:7181–6.
27. Penna D, Schmidt A, Beermann F. Tumors of the

retinal pigment epithelium metastasize to inguinal lymph nodes and spleen in tyrosinase-related protein 1/SV40T antigen transgenic mice. Oncogene 1998;17:2601–7.
28. Rousseau B, Dubayle D, Sennlaub F, et al. Neural and angiogenic defects in eyes of transgenic mice expressing a dominant-negative FGF receptor in the pigmented cells. Exp Eye Res 2000;71:394–04.
29. Kawase Y, Yanagi Y, Takato T, Fujimoto M, Okochi H. Characterization of multipotent adult stem cells from skin: transforming growth factor-β (TGF-β) facilitates cell growth. Exp Cell Res 2004;295:194–203.
30. Reiss M, Barcellos-Hoff MH. Transforming growth factor-β in breast cancer: a working hypothesis. Breast Cancer Res Treat 1997;45:81–95.
31. Reiss M. TGF-β and cancer. Microbes infect 1999;1:1327–47.
32. Samuels V, Barret JM, Bockman S, Pantazis CG, Allen MB, Jr. Immunocytochemical study of transforming growth factor-β expression in benign and malignant gliomas. Am J Pathol 1989;134:894–902.
33. Yamada N, Yamashita H, Nister M, et al. Enhanced expression of transforming growth factor-β and its type-I and type-II receptors in human glioblastoma. Int J Cancer 1995;62:386–92.
34. Annes JP, Munger JS, Rifkin DB. Making sense of latent TGFβ activation. J Cell Sci 2003;116:217–24.
35. Odeberg J, Piao JH, Samuelsson EB, Falci S, Akesson E. Low immunogenicity of *in vitro*-expanded human neural cells despite high MHC expression. J Neuroimmunol 2005;161:1–11.
36. Hori J, Ng TF, Shatos M, Klassen H, Streilein JW, Young MJ. Neural progenitor cells lack immunogenicity and resist destruction as allografts. Stem Cells 2003;21:405–16.
37. Armstrong RJ, Harrower TP, Hurelbrink CB, et al. Porcine neural xenografts in the immunocompetent rat: immune response following grafting of expanded neural precursor cells. Neuroscience 2001;106:201–16.
38. Nieda M, Nicol A, Denning-Kendall P, Sweetenham J, Bradley B, Hows J. Endothelial cell precursors are normal components of human umbilical cord blood. Br J Haematol 1997;98:775–7.
39. Marchetti S, Gimond C, Iljin K, et al. Endothelial cells genetically selected from differentiating mouse embryonic stem cells incorporate at sites of neovascularization *in vivo*. J Cell Sci 2002;115:2075–85.

Effect of Human Skin-Derived Stem Cells on Vessel Architecture, Tumor Growth, and Tumor Invasion in Brain Tumor Animal Models

Federica Pisati, Marzia Belicchi, Francesco Acerbi, et al.

Updated version	Access the most recent version of this article at: http://cancerres.aacrjournals.org/content/67/7/3054

Cited articles	This article cites 39 articles, 13 of which you can access for free at: http://cancerres.aacrjournals.org/content/67/7/3054.full#ref-list-1
Citing articles	This article has been cited by 1 HighWire-hosted articles. Access the articles at: http://cancerres.aacrjournals.org/content/67/7/3054.full#related-urls

E-mail alerts	Sign up to receive free email-alerts related to this article or journal.
Reprints and Subscriptions	To order reprints of this article or to subscribe to the journal, contact the AACR Publications Department at pubs@aacr.org.
Permissions	To request permission to re-use all or part of this article, use this link http://cancerres.aacrjournals.org/content/67/7/3054. Click on "Request Permissions" which will take you to the Copyright Clearance Center's (CCC) Rightslink site.